ARTICLES

Journal of Semiconductors
(2022) 43, 034102
doi: 10.1088/1674-4926/43/3/034102
JOS

Performance enhancement of solution-processed InZnO thin-film transistors by Al doping and surface passivation

Wensi Cai, Haiyun Li, Mengchao Li, and Zhigang Zang†

Key Laboratory of Optoelectronic Technology & System (Ministry of Education), Chongqing University, Chongqing 400044, China

Abstract: Solution-processed oxide semiconductors have been considered as a potential alternative to vacuum-based ones in printable electronics. However, despite spin-coated InZnO (IZO) thin-film transistors (TFTs) have shown a relatively high mobility, the lack of carrier suppressor and the high sensitivity to oxygen and water molecules in ambient air make them potentially suffer issues of poor stability. In this work, Al is used as the third cation doping element to study the effects on the electrical, optoelectronic, and physical properties of IZO TFTs. A hydrophobic self-assembled monolayer called octadecyltrimethoxysilane is introduced as the surface passivation layer, aiming to reduce the effects from air and understand the importance of top surface conditions in solution-processed, ultra-thin oxide TFTs. Owing to the reduced trap states within the film and at the top surface enabled by the doping and passivation, the optimized TFTs show an increased current on/off ratio, a reduced drain current hysteresis, and a significantly enhanced bias stress stability, compared with the untreated ones. By combining with high-capacitance AlO_x, TFTs with a low operating voltage of 1.5 V, a current on/off ratio of > 10^4 and a mobility of 4.6 $cm^2/(V{\cdot}s)$ are demonstrated, suggesting the promising features for future low-cost, low-power electronics.

Key words: thin-film transistors; oxide semiconductors; Al doping; surface passivation

Citation: W S Cai, H Y Li, M C Li, and Z G Zang, Performance enhancement of solution-processed InZnO thin-film transistors by Al doping and surface passivation[J]. *J. Semicond.*, 2022, 43(3), 034102. https://doi.org/10.1088/1674-4926/43/3/034102

1. Introduction

Ever since the first report of amorphous InGaZnO (IGZO) thin-film transistors (TFTs) in 2004 by Hosono *et al.* amorphous oxide semiconductors have received much attention owing to their excellent electrical properties[1, 2]. Out of all the deposition methods, solution-based techniques, such as spin-coating and ink-jet printing are considered as promising methods for the fabrication of TFTs because of their low-cost, easy integration with printable electronics and no requirement for high vacuum and high pressure[3]. However, TFTs deposited by solution-based methods generally show a poorer device performance than vacuum-based ones.

InZnO (IZO) is considered as a promising n-type oxide semiconductor since it can be easily deposited through a solution process while maintaining a relatively high mobility under amorphous states. We have previously reported that by modifying the annealing temperature of solution-processed IZO TFTs, it is able to achieve a high mobility approaching 10 $cm^2/(V{\cdot}s)$ and a high current on/off ratio[4]. However, such devices show a turn-on voltage less than 0 V, which is not ideal for circuit applications. Also, the lack of carrier suppressor might result in a poor bias stress stability of the devices. To solve such issues, elements such as Ga, B, and Al could be incorporated into oxide semiconductors to suppress the generation of oxygen vacancies[5–7]. Out of those materials, Al is highly desirable owing to the low cost and the strong bonding between Al and O[8]. By co-sputtering Al with IZO, Reed *et al.* reported Al-doped IZO (IZO:Al) TFTs and studied the effects of Al incorporation on the film and device performance[8]. However, to date, the reports on Al doping in solution-processed IZO TFTs are rare. Hence, a study on the effectiveness of Al doping in solution-processed oxide TFTs and a systematical investigation on the working mechanism is desirable.

Also, unlike Si and organic semiconductors, the top channel surface of oxide TFTs is extremely sensitive to air with water and -OH species being easily adsorbed on the top surface, resulting in a degraded device performance, particularly for those with an ultra-thin channel layer[9]. To solve such an issue, some treatments at the top surface are generally required to avoid direct contact with ambient air and passivate traps. One effective passivation layer is self-assembled monolayers (SAMs), which are solution-processable and plasma-damage-free to the underneath oxide semiconductors. Also, SAMs are chemically bonded onto the oxide films, meaning a good interface coupling is formed between the channel layer and the SAM, ensuring a good chemical stability[9, 10]. For applications such as backplane drivers for flat plane displays, good stability under operating conditions is essential. The instability of an oxide TFT is related to the traps at dielectric/channel interface, within the oxide film and at the top channel surface. SAM encapsulation can help improving the stability of oxide TFTs due to reduced top surface traps, as reported in several previous works[9, 11]. However, those works mainly focus on oxide semiconductors deposited using vacuum-based methods, and unlike those, solution-processed oxide TFTs generally show a poor device performance due to traps/defects within the film. Therefore, it is of great interest to study whether SAM encapsulation could work with the doping strategy to further improve the device performance.

Correspondence to: Z G Zang, Email: zangzg@cqu.edu.cn
Received 17 DECEMBER 2021; Revised 3 NOVEMBER 2021.
©2022 Chinese Institute of Electronics

In this work, we explored the possibility of the performance enhancement in solution-processed IZO TFTs by doping and surface passivation. Electrical, optoelectronic and physical properties of TFTs were systematically studied in order to analysis the mechanism of Al doping and octadecyltrimethoxysilane (OTES) SAM top surface passivation. Due to reduced traps within the films and at the top surface, a significantly enhanced device performance was achieved, including an increased current on/off ratio, a reduced hysteresis and, most importantly, an improved bias stress stability. The combination of this optimized IZO:Al with high capacitance AlO_x also enabled the demonstration of low-voltage TFTs, showing a mobility of 4.6 $cm^2/(V\cdot s)$ and a current on/off ratio of > 10^4. The work might have potential implications in future high-performance, low-cost optoelectronic devices such as transparent displays.

2. Experimental procedures

2.1. Solutions

To prepare Al-doped IZO precursors, first, aluminium nitrate nonhydrate ($Al(NO_3)_3\cdot 9H_2O$, 99.997%, Sigma), indium nitrate hydrate ($In(NO_3)_3\cdot xH_2O$, 99.99% Sigma), zinc nitrate hydrate ($Zn(NO_3)_2\cdot xH_2O$, 99.999%, Sigma) were separately dissolved in 2-Methoxyethanol (2-ME, 99%, Adamas) to yield solutions with a concentration of 0.2 M and stirred at room temperature for 24 h. Then the solutions were mixed together at a volume ratio of 0 : 50 : 50, 1 : 49.5 : 49.5, 3 : 48.5 : 48.5 and 5 : 47.5 : 47.5 for $Al(NO_3)_3$: $In(NO_3)_3$: $Zn(NO_3)_2$, respectively. The mixed solutions were stirred at room temperature for another 24 h and filtrated through 0.22 μm PTFE hydrophilic filters before use.

SAM solutions with a molar concentration of 0.01 M were prepared by adding octadecyltrimethoxysilane (OTES, 90%, Sigma) into toluene.

AlO_x precursors were prepared by dissolving $Al(NO_3)_3\cdot 9H_2O$ into 2-ME to yield solutions with a concentration of 0.3 M. The solution was then stirred at room temperature for 24 h and filtrated through 0.22 μm PTFE hydrophilic filters before use.

2.2. Device fabrication

Approximately 33 nm thick AlO_x films were deposited by spinning the precursor solutions at 2000 rpm for 35 s, followed by an immediate annealing at 120 °C for 1 min and another 1 h annealing at 350 °C in air.

To fabricate Al-doped IZO TFTs, first, precursors with different Al doping percentages were spin-coated on 100 nm thick SiO_2 or AlO_x films at 3000 rpm for 30 s, followed by an immediate annealing at 120 °C for 1 min and another 1 h annealing at 350 °C in air. Similar to what were reported previously, an intermediate annealing was done here in order to remove the residual solvent and/or rearrange the constituent elements within the layer[12, 13]. The films are measured to be 12.37 ± 0.15, 12.45 ± 0.02, 12.64 ± 0.04 and 13.45 ± 0.18 nm for Al doping percentages of 0%, 1%, 3% and 5%, respectively. Then 80 nm thick Al source/drain contacts were thermally evaporated on the film through shadow masks with a channel width-to-length ratio of 1500 : 80. Finally, the devices were dipped into SAM solutions for 3 h and then annealed in air at 105 °C for 20 min.

2.3. Measurement and characterization

The hall mobility and carrier concentration of the IZO:Al films were measured at room temperature using a PhysTech RH2035 Hall System. The absorbance of the films was measured using an UV-VIS-NIR Spectrophotometer (Shimadu UV-3600). X-ray photoelectron spectroscopy (XPS) of the films was measured on a Thermo ESCALAB 250 Xi with Al Kα emission at 1486.6 eV. The surface morphology of the film was measured using an Asylum Research atomic force microscope (AFM). The electrical performance of the devices was measured using a Keithley 4200SCS semiconductor analyzer.

The turn-on voltage, V_{on}, of TFTs is defined as the gate voltage, V_G, at which drain current, I_D, starts to increase in the I_D–V_G plot. The threshold voltage, V_{TH}, in the saturation region is extracted from the linear extrapolation of the value of V_G when $I_D = 0$ from $I_D^{1/2}$–V_G plot[2, 14].

3. Results and discussions

Fig. 1(a) shows the hall mobility as well as the carrier concentration of the IZO:Al films with different Al doping percentages. With the increase of Al addition from 0% to 5%, the hall mobility of the films drops from 9.4 to 3.2 $cm^2/(V\cdot s)$, suggesting that the addition of Al into the IZO films suppresses the carrier generation and decreases the carrier concentration.

The absorbance spectra of the IZO:Al films with different doping percentages are shown in Fig. 1(b), from which the bandgap of the films can be calculated using

$$\alpha h v = \left(h v - E_g\right)^{1/2}, \quad (1)$$

where α is the optical absorption coefficient, h is the Planck's constant, v is the frequency of light and E_g is the bandgap of the films. The inset of Fig. 1(b) shows the relationship between $(\alpha h v)^2$ and hv, from which bandgaps of 3.46, 3.52, 3.6, and 3.64 eV can be obtained for films doped with 0%, 1%, 3%, and 5% Al, respectively. An increase of bandgap is found here with the increase of Al doping percentages, suggesting a suppression of carrier concentration, which is in agreement with the results from Hall measurement.

The surface morphology of IZO:Al films is shown in Figs. 1(c)–1(f). The root-mean-square (RMS) roughness is found to be 1.83, 0.57, 0.59 and 0.73 nm for doping percentages of 0%, 1%, 3% and 5%, respectively. The doped films show a lower RMS roughness than undoped ones, which is attributed to the reduced trap states and surface modification by Al doping. With the films being amorphous for all the cases, the slight increase of RMS roughness at higher doping percentages might be caused by the aggregation of metal ions and generation of pinholes[15]. Generally, a smoother surface is preferred for suppressing both interface traps and scattering centres[15, 16].

The XPS spectra of all films were then studied, as shown in Fig. 2 and Fig. S1. All films show In peaks at 444.2 and 451.8 eV, and Zn peaks at 1021.4 and 1044.3 eV (Fig. S1), demonstrating the existence of metal-oxide bonds[17]. The atomic percentages of In, Zn, O and Al are found to be 24.3%, 39.9%, 35.8% and 0%, 25.4%, 41%, 33.2% and 0.4%, 24.9%, 40.3%, 34.2% and 0.6%, and 25.2%, 39.4%, 34.7% and 0.7% for films doped with 0%, 1%, 3% and 5% Al, respectively. As shown in Fig. 2, three peaks are found in the O 1s

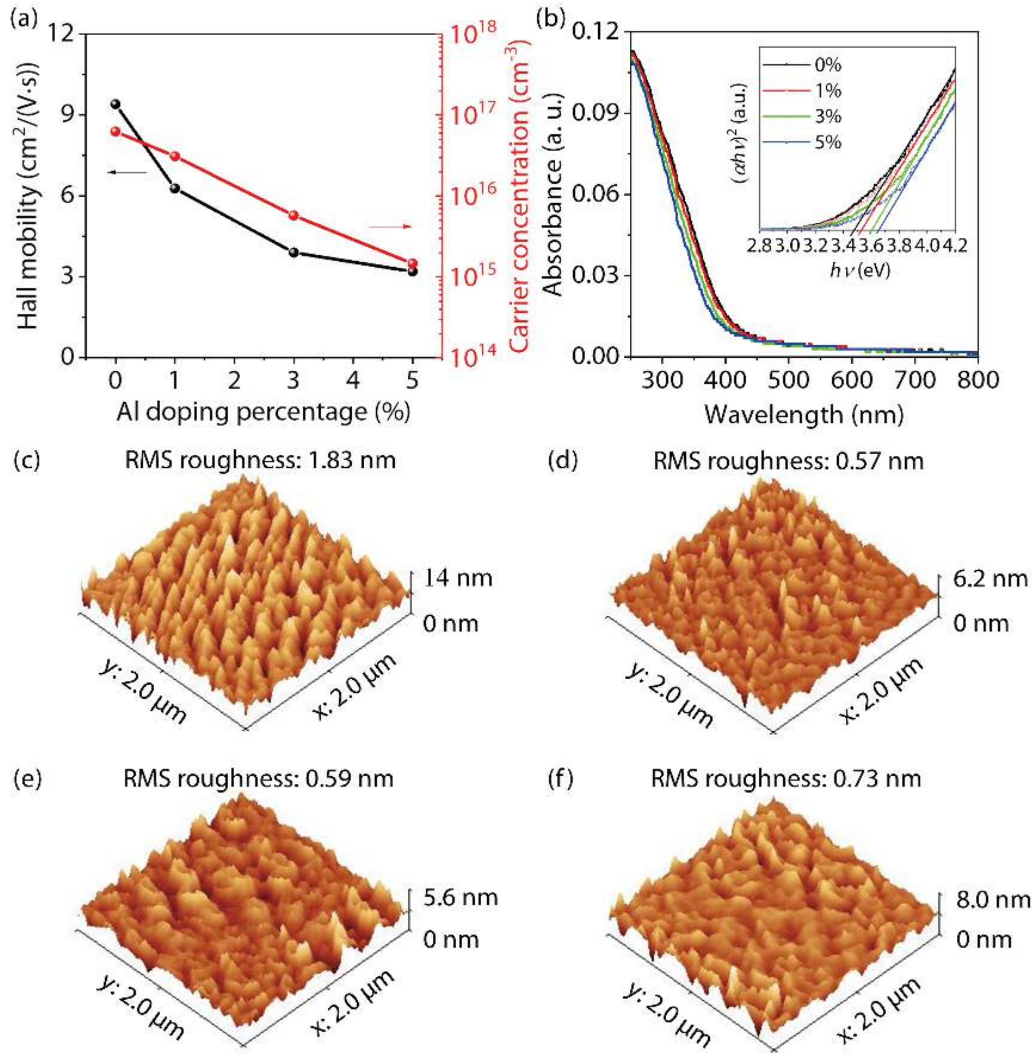

Fig. 1. (Color online) (a) Hall mobility and carrier concentration of the IZO:Al films. (b) Absorbance and corresponding bandgap (inset) of the IZO:Al films. Surface morphology of IZO films doped with (c) 0%, (d) 1%, (e) 3% and (f) 5% Al.

spectra, which are oxygen in the oxide lattices without oxygen vacancies (M-O-M, located at ~529.5 eV) and with oxygen vacancies (V_O, located at ~531.2 eV), and oxygen in the hydroxide (M-OH, located at ~532.5 eV)[18]. Oxygen vacancies are found to decrease with the increase of Al doping percentages. This is considered mainly due to the slightly larger electronegativity difference between Al (1.61) and O (3.44) than that with Zn (1.65) and In (1.78), making Al^{3+} ions have a stronger bond with O^{2-} than Zn^{2+} and In^{3+} ions. This is also in agreement with the Hall measurement, where carrier concentration and hall mobility also reduce with the increase of Al doping percentages, since vacancies are the source of free carriers. Both oxygen vacancies and -OH groups might work as traps at dielectric/channel interface and/or within the channel layer. The ratio of deficiencies within the film can be calculated using (V_O + M-OH)/(V_O + M-O-M + M-OH), and is found to be 50.7%, 48.4%, 52% and 52.2% for films with 0%, 1%, 3% and 5% Al dopants, respectively. This suggests that although Al doping can suppress the generation of oxygen vacancies, excess Al doping might increase the scattering centres due to excess Al source and/or create the defect by incomplete dehydration of excess $Al(OH)_3$[19, 20].

To study the effects of Al doping on device performance, IZO:Al (0%, 1%, 3% and 5%) TFTs were fabricated, as shown in Fig. 3(a) and summarized in Table 1. With the increase of Al doping percentages from 0 to 5%, the transfer characteristics shift toward positive and the mobility decrease, which might be caused by the higher bonding energy of Al–O (5.31 eV/512.1 kJ/mol) than that of In–O (3.59 eV/346 kJ/mol) and Zn–O (2.94 eV/284.1 kJ/mol)[21–23]. Also, the increase of bandgap could lead to a decrease in electron concentration and hence a reduction of mobility. Although I_D slightly increases with V_G being more negative due to the increase of leakage current induced by the electric field increment, for all TFTs, I_D remains at a low level of less than 1 nA in the off-states, which is far less than the on-current. A decrease of on- and off-current are found with the increase of doping percentages, which might be also the result of decreased electron concentration. Nevertheless, an increase of current on/off ratio is still achieved for the doped devices with the highest current on/off ratio of ~10^7 being achieved in TFTs doped with 1% Al. The total trap density, D_{total}, can be calculated using the subthreshold swing, SS, according to

$$D_{\text{total}} = \left[\frac{\text{SS}\log(e)}{\frac{kT}{q}} - 1\right]\frac{C}{q^2}, \tag{2}$$

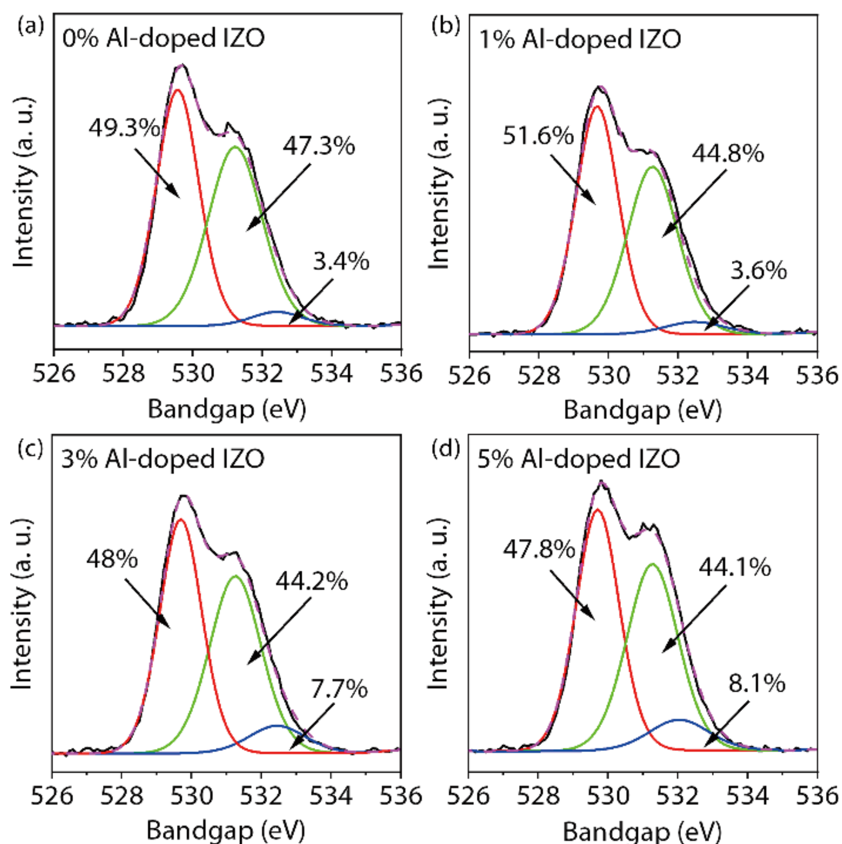

Fig. 2. (Color online) O 1s spectra of IZO:Al films doped with (a) 0%, (b) 1%, (c) 3% and (d) 5% Al.

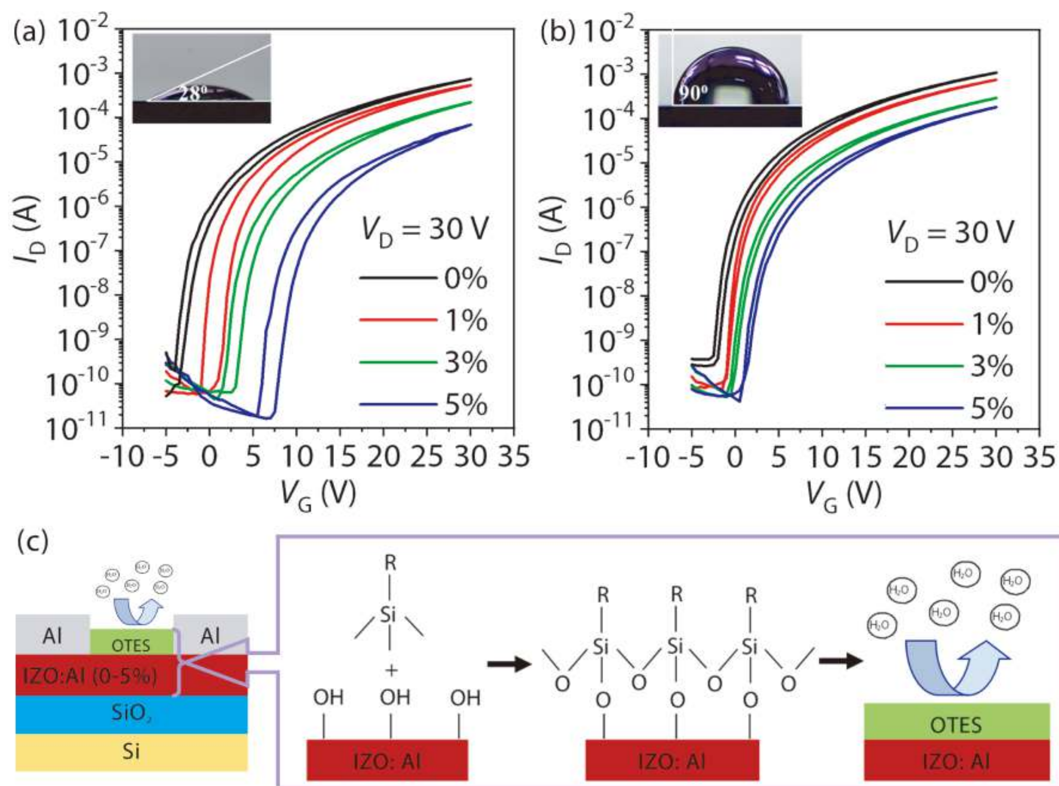

Fig. 3. (Color online) Transfer characteristics of IZO:Al TFTs (a) without and (b) with an OTES top surface treatment. The insets show images of a water drop on the surface of the IZO:Al films. (c) Schematic diagrams of TFT structures and OTES formation on IZO:Al surface. R represents $C_{18}H_{37}$.

where k is the Boltzmann constant, T is the temperature, and q is the electron charge. D_{total} is 2.38×10^{12}, 2.09×10^{12}, 2.27×10^{12} and 2.27×10^{12} $cm^{-2}eV^{-1}$ for TFTs doped with 0%, 1%, 3% and 5% Al, respectively. Lower D_{total} values are found in the doped TFTs, suggesting less traps existed at interface and/or within the film. The lowest D_{total} is found in TFTs

Table 1. Electrical properties of IZO:Al TFTs.

Al doping percentage	Treatment or not	Current on/off ratio (10^6)	V_{TH} (V)	SS (V/dec)	μ (cm²/(V·s))	D_{total} (10^{12} cm^{-2} eV^{-1})
0%	No	3.8	5.67	0.72	3.9	2.38
	Yes	4.1	5.5	0.61	5.6	1.98
1%	No	8	6.6	0.64	3.5	2.09
	Yes	10	6.35	0.57	4.2	1.84
3%	No	4.8	10.2	0.69	1.78	2.27
	Yes	4.8	7.97	0.59	1.87	1.91
5%	No	3.9	12.72	0.69	0.81	2.27
	Yes	4.3	9.24	0.6	1.32	1.95

doped with 1% Al, which is also in agreement with the film properties obtained from AFM and XPS measurements. D_{total} slightly increases at higher doping percentages (i.e., 3% and 5%), which might be due to the increase of scattering centres caused by the excess Al source and/or the creation of $Al(OH)_3$[19, 20].

In general, some water molecules from air might be easily adsorbed on the top channel surface of an oxide TFT and capture free electrons in the film through $2H_2O + O_2 + 4e^- \rightarrow 4OH^-$, resulting in a hydroxylated surface[9]. The adsorption and desorption of the water molecules at the surface could also lead to deleterious effects on the device performance. To avoid such issues, we treated the top surface of the TFTs with an OTES SAM, which could react with the -OH groups, desorb weakly adsorbed water molecules, and form a passivation layer to prevent any further adsorption of water (Fig. 3(c)). The formation of the hydrophobic protection layer is confirmed by the water contact angle, which increases from 28° to 90° owing to the treatment (insets of Figs. 3(a) and 3(b)). A schematic diagram of the treated TFTs is shown in Fig. 3(c), and their transfer characteristics and electrical performance are shown in Fig. 3(b) and Table 1. Compared with the untreated devices, a decrease of clockwise hysteresis is clearly seen. The charge trapping by the adsorbed water molecules on the oxide semiconductor surface has been reported as the main source for the hysteresis[24]. Hence, the remarkably reduced drain current hysteresis between forward and backward sweeps after the OTES treatment could be explained by the reduced trap states on the top surface. All devices show an increase of mobility and a left shift of threshold voltage, V_{TH}, after the treatment, which might be due to the desorption of weakly adsorbed water molecules and the release of trapped electrons. Decrease of SS and D_{total} are also found after the treatment. D_{total} is related to the dielectric/channel interface trap density, bulk trap density and top surface trap density, D_{top}[25]. Therefore, the decrease of SS after the OTES treatment could be explained by the decrease of the trap density from top surface. The reduction of D_{top} is calculated to be more than 12% of D_{total}, demonstrating that the top surface condition plays a crucial role in solution-processed, ultra-thin devices. Clearly, the treated 1% doped TFTs show the best overall device performance, including an increase of current on/off ratio by a factor of 2.6 and a reduction of trap density by 23% compared with the untreated IZO TFTs.

To test the effectiveness and reliability of Al doping and OTES treatment under operating conditions, bias stress stability of all TFTs were then studied, as shown in Figs. 4(a), 4(b), S2 and S3. While the devices without treatment show a large threshold voltage change of +4.58 V even only being positively biased at V_G = 30 V for 600 s (Fig. S2(a)), the threshold voltage change dramatically reduces after the treatment (Fig. S2(b)). Such an improvement is considered mainly due to the reduction of top surface traps, as water exposure could significantly increase the bias stress instability of TFTs[26, 27]. For the capped devices, the threshold voltage shift under bias stresses is considered mainly due to the traps (i.e., oxygen vacancies and -OH groups) at dielectric/channel interface and/or within the channel layer[28]. Fig. S3 shows that all devices have an insignificant change of SS due to bias stresses, indicating the creation of additional defect states at the dielectric/channel interface by the gate bias stress is negligible[29]. The best bias stress stability is achieved in 1% Al doped TFTs with a threshold voltage change of +1.47 and –1.41 V after being positively biased at V_G = 30 V or negatively biased at V_G = –30 V for 1800 s, respectively (Figs. 4(a) and 4(b)). Such a better stability as compared to other IZO:Al TFTs is considered mainly due to the better film quality with less traps/defects existed in the film, as confirmed by the XPS and AFM measurements. Notably, the stability of the devices is found to first become better with the doping of Al, but then get worse with further increment of doping percentages, showing an even worse stability than the undoped one when increasing the doping percentage to 5%. The XPS results suggest that the area ratio of M-OH increases at higher doping percentages, hence the worse stability might be related to the trapped electrons by the additional defects formed around Al atoms due to the incomplete dehydration of excess $Al(OH)_3$[19, 30].

The results clearly suggest that the optimized condition is obtained at a doping percentage of 1%. We therefore study the long-term stability of 0% and 1% Al doped IZO TFTs, as shown in Figs. 4(c) and 4(d). Both TFTs show a reasonably good long-term stability, with fairly small changes of device performance even after being stored in ambient air for 4 months. Nevertheless, a smaller change is found in 1% doped case, with a threshold voltage change of only +0.11 V after the 4 months' storage as compared to a change of +0.97 V for the undoped case. Such an improvement in the long-term stability is considered as the result of the improved film properties and/or the reduced trap states at the dielectric/channel interface due to doping since the doped TFTs show a lower total trap density.

For battery-powered portable electronics, a lower operating voltage could give a lower power consumption and hence a longer time of use without recharging. However, until now it is still quite challenging to achieve oxide TFTs with both a reasonably high current on/off ratio and a low operating voltage. Besides, the increasing need on printable electron-

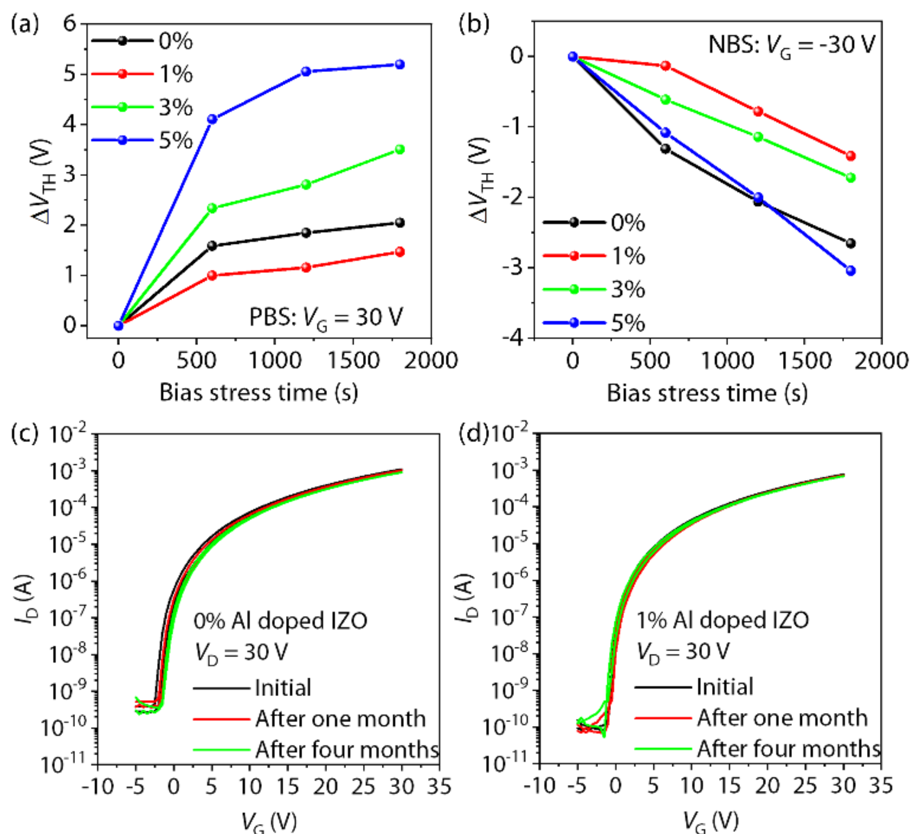

Fig. 4. (Color online) Threshold voltage shift of IZO:Al TFTs under (a) a positive bias stress (PBS) and (b) a negative bias stress (NBS). Transfer characteristics of (c) 0% and (d) 1% Al doped IZO TFTs before and after being stored in ambient air for 4 months.

ics has led the attention on fully solution-processed TFTs. However, compared with their vacuum-deposited counterparts, solution-processed oxide TFTs generally show a poorer device performance, especially under a low operating voltage. To lower the operating voltage, here solution-processed AlO_x films are used, which have a high gate capacitance of 143 nF/cm^2. With a thickness of 32.95 ± 0.11 nm being measured for the film, this corresponds to a dielectric constant of 5.32. Such a value is lower than the theoretical value of Al_2O_3, which might be due to the formation of highly polar $Al(OH)_3$ in the film[31]. The films also show a low current density less than 50 nA/cm^2 over an applied voltage range of −2 to 2 V (Fig. 5(a)). The surface morphology of the film is shown in Fig. 5(b). The film shows a continuous coverage with negligible porosity and an RMS roughness of 0.2 nm, which is considered suitable for TFT applications.

With the use of such AlO_x layers and 1% Al-doped IZO films, solution-processed IZO:Al TFTs were then demonstrated. The output characteristics in Fig. 5(c) suggest that the TFTs work in an n-type enhancement mode with linear, pinch-off and saturation regions clearly seen. The corresponding transfer characteristics are shown in Fig. 5(d). Owing to the high gate capacitance of AlO_x, the TFTs show a low operating voltage of 1.5 V with a current on/off ratio of > 10^4, a mobility of 4.6 cm^2/(V·s) and a subthreshold swing of 0.17 V/dec. The devices also show a turn-on voltage very close to 0 V with a negligible hysteresis between forward and backward sweeps, which is promising for circuit applications. A total trap density of 1.6 × 10^{12} cm^{-2}eV^{-1} is calculated, which is either comparable to or even better than those with similar interfaces reported previously[32, 33], and is considered as the main reason for the high device performance. With a same annealing temperature being used for both AlO_x and IZO:Al layers, some diffusions might happen between dielectric and channel layers, resulting in an intersecting region at the dielectric/channel interface. When applying a positive gate voltage, the carriers must overcome the barriers to reach the interface between intersecting region and gate dielectric owing to the existence of this intersecting region, resulting in a low mobility and on-current[34]. The wide intersecting region might also reduce the effective gate potential, causing a decrement of accumulated carriers at the intersecting region/channel interface and a further lowering of the mobility and on-current[34]. Nevertheless, our TFTs still show a reasonably high device performance, as summarized in Table 2. The comparison with other representative low-voltage, solution-processed oxide TFTs suggests that our device performance is comparable to or even better than those reported previously, demonstrating the great potential of our devices in future low-cost, low-power electronics.

4. Conclusion

In conclusion, we studied the influence of Al addition and OTES treatment on the electrical, optoelectronic and physical properties of solution-processed IZO TFTs. Compared with pure IZO TFTs, optimized IZO:Al TFTs exhibited a significantly enhanced electrical performance, including an increase of current on/off ratio by a factor of 2.6 and a reduction of trap density by more than 23%. Such a hugely reduced trap density also dramatically improved the bias stress stability. Fully solution-processed IZO:Al TFTs were demonstrated, showing a low operating voltage of 1.5 V, a current on/off ratio of

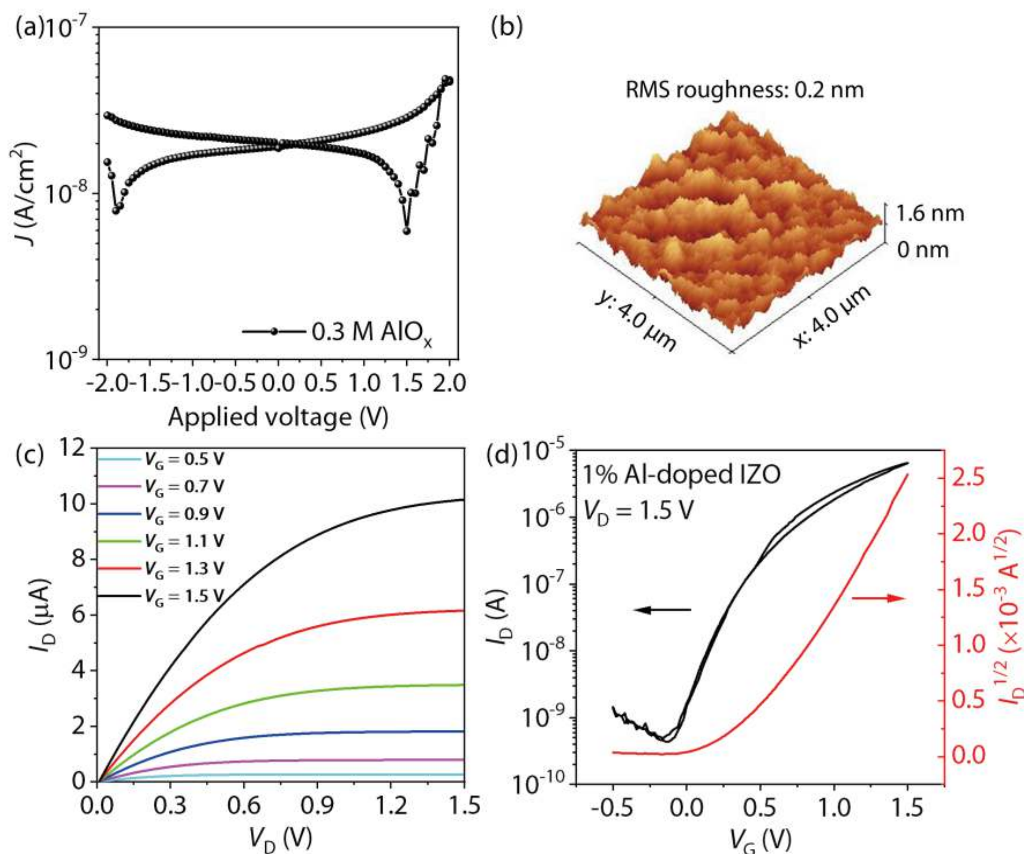

Fig. 5. (Color online) (a) Current density as a function of applied voltage for Si/AlO_x/Al capacitors. (b) Surface morphology of AlO_x. (c) Output and (d) transfer characteristics of low-voltage IZO:Al TFTs.

Table 2. Electrical performance of low-voltage, solution-processed oxide TFTs.

μ (cm²/(V·s))	V_G range (V)	V_{ON} (V)	I_{ON}/I_{OFF}	V_{TH} (V)	SS (V/dec)	D_{total} (10^{12} cm^{-2}eV^{-1})	Ref.
4.6	−0.5 to 1.5	−0.08	1.4×10^4	0.5	0.17	1.6	This work
0.06	−0.5 to 1	−0.3	$>10^5$	0.2	0.085	12	[33]
0.15	−0.5 to 1	−0.25	$\sim10^4$	0.0013	/	/	[35]
3.2	−1 to 2	0.18	10^6	/	0.073	/	[36]
7.23	−1 to 3	0	3.06×10^6	1.32	/	/	[37]
13.4	−1 to 3	−0.7	$>10^5$	0.44	/	/	[38]
1.05	−5 to 5	0.2	10^7	0.18	0.105	/	[39]
5.48	−2 to 6	/	10^7	0.72	0.33	9	[40]

$> 10^4$, and a mobility of 4.6 cm²/(V·s). The reported work demonstrates a convenient and yet effective method to substantially improve the performance of solution-processed oxide TFTs, which might have potential applications in future low-cost, low-power printable electronics.

Acknowledgements

We thank the National Natural Science Foundation of China (11974063), China Postdoctoral Science Foundation (2020M683242), and Chongqing Special Postdoctoral Science Foundation (cstc2020jcyj-bshX0123) for financial support.

Appendix A. Supplementary material

Supplementary data associated with this article can be found, in the online version, at https: //doi.org/10.1088/1674-4926/43/3/034102.

References

[1] Nomura K, Ohta H, Takagi A, et al. Room-temperature fabrication of transparent flexible thin-film transistors using amorphous oxide semiconductors. Nature, 2004, 432, 488

[2] Fortunato E, Barquinha P, Martins R. Oxide semiconductor thin-film transistors: a review of recent advances. Adv Mater, 2012, 24, 2945

[3] Park J W, Kang B H, Kim H J. A review of low-temperature solution-processed metal oxide thin-film transistors for flexible electronics. Adv Funct Mater, 2020, 30, 1904632

[4] Cai W, Li H, Zang Z. One-volt, solution-processed InZnO thin-film transistors. IEEE Electron Device Lett, 2021, 42, 525

[5] Park W J, Shin H S, Ahn B D, et al. Investigation on doping dependency of solution-processed Ga-doped ZnO thin film transistor. Appl Phys Lett, 2008, 93, 083508

[6] Zhong D Y, Li J, Zhou Y H, et al. The material properties of novel boron doped InZnO thin films by solution process and its application in thin film transistors with enhanced thermal stability. Super-

lattices Microstruct, 2018, 122, 377

[7] Jeon H J, Maeng W J, Park J S. Effect of Al concentration on the electrical characteristics of solution-processed Al doped ZnSnO thin film transistors. Ceram Int, 2014, 40, 8769

[8] Reed A, Stone C, Roh K, et al. The role of third cation doping on phase stability, carrier transport and carrier suppression in amorphous oxide semiconductors. J Mater Chem C, 2020, 8, 13798

[9] Cai W, Wilson J, Zhang J, et al. Significant performance enhancement of very thin InGaZnO thin-film transistors by a self-assembled monolayer treatment. ACS Appl Electron Mater, 2020, 2, 301

[10] Cai W, Zang Z, Ding L. Self-assembled monolayers enhance the performance of oxide thin-film transisotrs. J Semicond, 2021, 42, 030203

[11] Zhong W, Li G, Lan L, et al. InSnZnO thin-film transistors with vapor-phase self-assembled monolayer as passivation layer. IEEE Electron Device Lett, 2019, 39, 1680

[12] Nayak P K, Hedhili M N, Cha D, et al. Impact of soft annealing on the performance of solution-processed amorphous zinc tin oxide thin-film transistors. ACS Appl Mater Interfaces, 2013, 5, 3587

[13] Kim Y G, Kim T, Avis C, et al. Stable and high-performance indium oxide thin-film transistor by Ga doping. IEEE Trans Electron Devices, 2016, 63, 1078

[14] Cai W, Wilson J, Song A. Present status of electric-double-layer thin-film transistors and their applications. Flex Print Electron, 2021, 6, 043001

[15] Kim D N, Kim D L, Kim G H, et al. The effect of La in InZnO systems for solution-processed amorphous oxide thin-film transistors. Appl Phys Lett, 2010, 97, 192105

[16] Bukke R N, Saha J K, Mude N N, et al. Lanthanum doping in zinc oxide for highly reliable thin-film transistors on flexible substrates by spray pyrolysis. ACS Appl Mater Interfaces, 2020, 12, 35164

[17] Choi J, Park J, Lim K H, et al. Photosensitivity of InZnO thin-film transistors using a solution process. Appl Phys Lett, 2016, 109, 132105

[18] Lee K H, Park J H, Yoo Y B, et al. Effects of solution temperature on solution-processed high-performance metal oxide thin-film transistors. ACS Appl Mater Interfaces, 2013, 5, 2585

[19] Zhong D, Li J, Zhao C, et al. Enhanced electrical performance and negative bias illumination stability of solution-processed InZnO thin-film transistor by boron addition. IEEE Trans Electron Devices, 2018, 65, 520

[20] Li J, Huang C X, Fu Y Z, et al. Amorphous LaZnSnO thin films by a combustion solution process and application in thin film transistors. Electron Mater Lett, 2016, 12, 76

[21] Yang C, Li Y, Li J. Ab initio total energy study of ZnO adsorption on a sapphire (0001) surface. Phys Rev B, 2004, 70, 045413

[22] Wang D, Jiang J, Furuta M. Investigation of carrier generation mechanismin fluorine-doped n^+-In –Ga –Zn –O for self-aligned thin-film transistors. J Display Technol, 2016, 12, 258

[23] Luo Y R. Comprehensive handbook of chemical bond energies. CRC Press, 2007

[24] Xu W, Liu D, Wang H, et al. Facile passivation of solution-processed InZnO thin-film transistors by octadecylphosphonic acid self-assembled monolayers at room temperature. Appl Phys Lett, 2014, 104, 173504

[25] Shao L, Nomura K, Kamiya T, et al. Operation characteristics of thin-film transistors using very thin amorphous In–Ga–Zn–O channels. Electrochem Solid St Lett, 2011, 14, H197

[26] Lopes M E, Gomes H L, Medeiros M C R, et al. Gate-bias stress in amorphous oxide semiconductors thin-film transistors. Appl Phys Lett, 2009, 95, 063502

[27] Jeong J K, Won Yang H, Jeong J H, et al. Origin of threshold voltage instability in indium-gallium-zinc oxide thin film transistors. Appl Phys Lett, 2008, 93, 123508

[28] Jeong Y, Bae C, Kim D, et al. Bias-stress-stable solution-processed oxide thin film transistors. ACS Appl Mater Interfaces, 2010, 2, 611

[29] Suresh A, Muth J F. Bias stress stability of indium gallium zinc oxide channel based transparent thin film transistors. Appl Phys Lett, 2008, 92, 033502

[30] Choi W S, Jo H, Kwon M S, et al. Control of electrical properties and gate bias stress stability in solution-processed a-IZO TFTs by Zr doping. Curr Appl Phys, 2014, 14, 1831

[31] Cai W, Park S, Zhang J, et al. One-volt IGZO thin-film transistors with ultra-thin, solution-processed Al_xO_y gate dielectric. IEEE Electron Device Lett, 2018, 39, 375

[32] Lan L, Peng J. High-performance indium–gallium–zinc oxide thin-film transistors based on anodic aluminum oxide. IEEE Trans Electron Devices, 2011, 58, 1452

[33] Mukherjee A, Ottapilakkal V, Sagar S, et al. Ultralow-voltage field-effect transistors using nanometer-thick transparent amorphous indium–gallium–zinc oxide films. ACS Appl Nano Mater, 2021, 4, 8050

[34] Ning H, Zhou S, Cai W, et al. Fabrication of high-performance solution processed thin film transistors by introducing a buffer layer. Appl Surf Sci, 2020, 504, 144360

[35] Ko J, Kim J, Park S Y, et al. Solution-processed amorphous hafnium-lanthanum oxide gate insulator for oxide thin-film transistors. J Mater Chem C, 2014, 2, 1050

[36] Moreira M, Carlos E, Dias C, et al. Tailoring IGZO composition for enhanced fully solution-based thin film transistors. Nanomaterials, 2019, 9, 1273

[37] Xia W, Xia G, Tu G, et al. Sol-gel processed high-k aluminum oxide dielectric films for fully solution-processed low-voltage thin-film transistors. Ceram Int, 2018, 44, 9125

[38] Zhang Q, Ruan C, Xia G, et al. Low-temperature solution-processed InGaZnO thin film transistors by using lightwave-derived annealing. Thin Solid Films, 2021, 723, 138594

[39] Avis C, Kim Y G, Jang J. Solution processed hafnium oxide as a gate insulator for low-voltage oxide thin-film transistors. J Mater Chem, 2012, 22, 17415

[40] Jiang G, Liu A, Liu G, et al. Solution-processed high-k magnesium oxide dielectrics for low-voltage oxide thin-film transistors. Appl Phys Lett, 2016, 109, 183508

Wensi Cai received her PhD degree from University of Manchester in 2019. She joined Chongqing University as a postdoc researcher since 2020. Her research interests mainly focus on oxide semiconductor- and perovskite-based electron devices.

Zhigang Zang received his PhD degree from Kyushu University in 2011. He joined the School of Optoelectronic Engineering, Chongqing University, as a professor since 2014. His research interests mainly focus on the synthesis of II–VI, III–V semiconductor materials and their applications in solar cells, photodetectors and light emitting diodes.